Proceedings of the 10th Brazilian Congress of Thermal Sciences and Engineering – ENCIT 2004
Braz. Soc. of Mechanical Sciences and Engineering – ABCM, Rio de Janeiro, Brazil, Nov. 29 – Dec. 03, 2004

Paper CIT04-0844

STABILITY OF THE CHEMICAL AND HYDRODYNAMIC FIELDS CLOSE TO A ROTATING DISK ELECTRODE

J. Pontes
Metallurgy and Materials Engineering Department/EP-COPPE – Federal University of Rio de Janeiro
PO Box 68505 21941-972 Rio de Janeiro RJ, Brazil
jopontes@ufrj.br

N. Mangiavacchi
Mechanical Engineering Department, State University of Rio de Janeiro
R. São Francisco Xavier 524 20550-013 Rio de Janeiro, RJ, Brazil
norberto@uerj.br

O. E. Barcia
Institute of Chemistry/IQ – Federal University of Rio de Janeiro
PO Box 68505 21941-972 Rio de Janeiro RJ, Brazil
barcia@metalmat.ufrj.br

O. R. Mattos
Metallurgy and Materials Engineering Department/EP-COPPE – Federal University of Rio de Janeiro
PO Box 68505 21941-972 Rio de Janeiro RJ, Brazil
omattos@metalmat.ufrj.br

B. Tribollet
UPR15 – CNRS, Physique des Liquides et Electrochimie
4 place Jussieu, 75252 Paris Cedex 05, France
bt@ccr.jussieu.fr

Abstract. *Polarization curves experimentally obtained in the electro-dissolution of iron in a 1* **M** $\mathbf{H_2SO_4}$ *solution using a rotating disk as the working electrode present a current instability region within the range of applied voltage in which the current is controlled by mass transport in the electrolyte. According to the literature (Barcia, 1992) the electro-dissolution process leads to the existence of an axial viscosity gradient in the interface metal-solution, which leads to a deviation from von Kármán's classical solution for rotating disk flow. On two previous papers, Pontes et al (J. of the Braz. Soc. Mechanical Sciences, Vol. XXIV, pp. 139, 2002, and Phys. of Fluids, Vol. 16, No. 3, pp. 707, 2004) showed that stability of the steady flow, affected by a time-independent viscosity gradient pointing in the axial directions, is strongly affected by the stratified viscosity profile. In this work, we go one step beyond, by considering the stability of the hydrodynamic field, coupled through the viscosity, to the chemical field originated by the transport of one species. A phenomenological law is assumed, relating the viscosity to the concentration of chemical species. The steady state of the problem is obtained and a linear stability analysis of the coupled fields is made. The resulting eigenvalue-eigenfuction problem is presented, as well as some neutral stability curves.*

keywords: *Rotating Disk, Hydrodynamic Stability, Electrochemistry*

1. Introduction

Electrochemical cells using a rotating disk electrode are a widely used experimental tool in electrochemistry, due the simplicity of the setup and the fact that the mass flux is independent of the radial position along the disk, at steady state conditions (Levich, 1962). Furthermore, the rate of transfer of ions close of the electrode is conveniently controlled by imposing an adequate angular velocity to the electrode. This rate of transfer defines the maximum steady state current attained in an experiment.

Two current instabilities are observed in the region where the current is controlled by mass transport (Ferreira et al., 1994). The first instability is intrinsic to the system, while the current instability close to the active-passive transition is affected by the output impedance of the control equipment. This instability can be suppressed by using a negative feedback resistance (Epelboin et al., 1979), that gives rise to a continuous transition.

Most explanations presented in the literature for the current instabilities are based on mechanisms proposing a $\mathbf{FeSO_4}$ film precipitated at the electrode surface (Russel and Newman, 1986). In fact, changes in the ohmic voltage drop due to precipitation and dissolution of a $\mathbf{FeSO_4}$ film provide an acceptable explanation for the instability observed in the active/passive transition region, coupled with the output impedance of the control equipment. However, this model can not be generalized to explain oscillations observed at the beginning of the current plateau. Indeed, using electro-hydrodynamic (EHD) impedance measurements (Tribollet and Newman, 1983), Barcia *et al.* (Barcia et al., 1992) studied the electro-dissolution of iron electrodes in 1 $\mathbf{M}$ $\mathbf{H_2SO_4}$ at the current plateau, before and after the first instability region. They propose that the electro-dissolution process leads to the existence of a viscosity gradient in the diffusion boundary layer, which could affect the stability of the hydrodynamic field and explain the observed current instability.

To investigate the importance of the hydrodynamics in the electro-dissolution of iron, Ferreira *et al.* (Ferreira et al., 1994) and Geraldo *et al.* (Geraldo et al., 1998) studied the influence of the viscosity on the current oscillations observed at the beginning of the current plateau region of the above described experiment. These authors found that increasing the bulk electrolyte viscosity – and therefore decreasing the Reynolds number of the experiment – by adding glycerol to the solution, the current signals evolve from chaotic to periodic, and to a stationary regime, where the instability is suppressed. They also found that the current oscillations are enhanced by an increase in the angular velocity of the electrode.

The existence of a hydrodynamic instability in rotating disk flow has been the object of a number of investigations, both experimental and theoretical in the case of fluids with uniform viscosity. The main result shows that the steady flow becomes unstable beyond a certain non-dimensional distance from the axis of rotation.

The flow develops corotating vortices which spiral outward with their axes along logarithmic spirals of angle $90° + \varepsilon$ ($\varepsilon \approx 13°$) with respect to radius of the disk. Malik (Malik, 1986) determined the neutral stability curve for stationary vortex disturbances, which turn with the angular velocity of the disk. Neutral curves were presented in the $\alpha \times R$, $\beta \times R$ and $\varepsilon \times R$ planes for zero-frequency disturbances, where α and β are the components of the real perturbation wave-vector along the radial and azimuthal directions and ε is the angle between the perturbation and the radial direction, given by $\varepsilon = \tan^{-1} \beta/\alpha$. The critical Reynolds number was found to be in good agreement with experimental results, at a value of $R = 285.36$.

A comprehensive review of the literature on the subject, concerning research made until 1989 can be found in the paper by Reed and Saric (Reed and Saric, 1989).

Faller (Faller, 1991) determined the neutral stability curves for setup configurations consisting of rotating or stationary disks and flows approaching the disk with (rotating flow) or without (stationary flow) bulk angular velocity. Critical Reynolds number for the case of rotating disk and stationary fluid was found as 69.4.

Lingwood (Lingwood, 1995) presented the neutral curve for vortices turning with several angular velocities and theoretical results concerning the asymptotic response of the flow to an impulsive excitation exerted in the flow at a certain radius at $t = 0$. Additionally, Lingwood's work addresses the case where the wavenumber component along the radial direction, α, is complex, leading to an exponential growth along that direction. The curve for this case defines the region of absolute instability, with a critical Reynolds number of $R = 510.625$.

It is well known that boundary layers can be destabilized by increasing the viscosity close to the wall and stabilized by decreasing, through heating or cooling the wall (Schlichting and Gersten, 1999). Schäfer *et al.* (Schäfer et al., 1995) deduced an asymptotic expression for the critical Reynolds number for moderate temperature differences in boundary layers developed over flat plates, taking into account the temperature dependency of the viscosity. Turkyilmazoglu Cole and Gajjar (Turkyilmazoglu et al., 1998) studied the influence of heat transfer on the convective and absolute instability of compressible boundary layers in rotating disk flow.

On two previous papers, Pontes *et al.* (Pontes et al., 2002, Pontes et al., 2004) showed that stability of the steady flow, affected by a time-independent viscosity gradient pointing in the axial directions, is strongly affected by the stratified viscosity profile. In this work, we go one step beyond, by considering the stability of the hydrodynamic field, coupled through the viscosity, to the chemical field originated by the transport of one species. A phenomenological law is assumed, relating the viscosity to the concentration of chemical species. The steady state of the problem is obtained and a linear stability analysis of the coupled fileds is made. The resulting eigenvalue-eigenfuction problem is presented, as well as some neutral stability curves.

Four linear stability analysis are presented in this work. All four cases address the stability of base state with respect to perturbations turning with the angualr velocity of the rotating electrode. The first case, denoted as case No. 1, refers to fluids with constant viscosity (see Malik, 1986 and Pontes et al., 2004) and is presented for purposes of comparison with the new results. The three other cases refer to fluids with variable viscosity. Case No. 2 refers to problems with Schmidt number $Sc = 50$. This case is, in fact, not realistic since Schmidt numbers usualy found in the diffusion of chemical species in liquids are in the range of 1000 or larger. However, the case is presented in order to provide a better understanding on how the neutral curves change as this parameter increases. Cases Nos. 3 and 4 refer to problems with $Sc = 1000$ and 2000, respectively, the last one corresponding to the the Schmidt number found in the actual electrochemical problem. All variable viscosity

cases where studied assuming the same phenomenological law relating concentration of the relevant chemical species and fluid viscosiy, as discussed below.

2. The Base State

The steady hydrodynamic field coupled to the transport of a chemical species is an extension of the well known von Kármán (von Kármán and Angew, 1921) exact solution of the continuity and Navier-Stokes equations for laminar rotating disk-flow, written in a rotating coordinate frame turning with the disk angular velocity Ω.

The continuity, momentum, and concentration equations on a rotating frame are given by:

$$\mathbf{div}\,\mathbf{v} = 0 \tag{1}$$

$$\frac{D\mathbf{v}}{Dt} = -2\boldsymbol{\Omega}\times\mathbf{v} - \frac{1}{\rho}\,\mathbf{grad}\,p + \frac{1}{\rho}\,\mathbf{div}\,\tau \tag{2}$$

$$\frac{Dc}{Dt} = \mathbf{div}\,(D\,\mathbf{grad}\,c) \tag{3}$$

where τ is the Newtonian viscous stress tensor.

Assuming that the stationary chemical species concentration depends only on the axial direction, the stationary coupled fields are governed by:

$$\frac{\partial v_r}{\partial r} + \frac{v_r}{r} + \frac{\partial v_z}{\partial z} = 0 \tag{4}$$

$$v_r\frac{\partial v_r}{\partial r} - \frac{v_\theta^2}{r} + v_z\frac{\partial v_r}{\partial z} = 2\Omega v_\theta + \nu\left(\frac{2}{r}\frac{\partial}{\partial r}\left(r\frac{\partial v_r}{\partial r}\right) - \frac{2v_r}{r^2}\right) + \frac{\partial}{\partial z}\left(\nu\frac{\partial v_r}{\partial z}\right) \tag{5}$$

$$v_r\frac{\partial v_\theta}{\partial r} + \frac{v_r v_\theta}{r} + v_z\frac{\partial v_\theta}{\partial z} = -2\Omega v_r + \frac{\nu}{r^2}\frac{\partial}{\partial r}\left(r^3\mu\frac{\partial}{\partial r}\left(\frac{v_\theta}{r}\right)\right) + \frac{\partial}{\partial z}\left(\nu\frac{\partial v_\theta}{\partial z}\right) \tag{6}$$

$$v_r\frac{\partial v_z}{\partial r} + v_z\frac{\partial v_z}{\partial z} = -\frac{1}{\rho}\frac{\partial p}{\partial z} + \nu\left(\frac{1}{r}\frac{\partial}{\partial r}\left(r\frac{\partial v_r}{\partial z}\right) + 2\frac{\partial^2 v_z}{\partial z^2}\right) + 2\frac{\partial\nu}{\partial z}\frac{\partial v_z}{\partial z} \tag{7}$$

$$v_z\frac{\partial c}{\partial z} = \frac{\partial D}{\partial z}\frac{\partial c}{\partial z} + D\frac{\partial^2 c}{\partial z^2} \tag{8}$$

where c is the chemical species concentration and D is its diffusion coefficient in the electrochemical cell electrolite.

The steady solution takes the form:

$$\bar{v}_r = r\,\Omega\,F(z) \tag{9}$$

$$\bar{v}_\theta = r\,\Omega\,G(z) \tag{10}$$

$$\bar{v}_z = (\nu(\infty)\,\Omega)^{1/2}\,H(z) \tag{11}$$

$$\bar{p} = \rho\nu(\infty)\Omega P(z) \tag{12}$$

$$\bar{c} = C_\infty + (C_0 - C_\infty)C(z) \tag{13}$$

where $\nu(\infty)$ is the bulk viscosity, far from the electrode surface. Equations (9–13) are introduced in the dimensional continuity and Navier-Stokes equations. Defining the the bulk Schmidt number $Sc = \nu(\infty)/D(\infty)$, and the sensitivity factor $\gamma = \frac{1}{\nu(\infty)}\frac{d\nu}{dC}$ leads to the following system of equations for F, G, H and P:

$$2F + H' = 0 \tag{14}$$

$$F^2 - (G+1)^2 + HF' = \nu^*F'' + \gamma F'C' \tag{15}$$

$$2F(G+1) + HG' = \nu^*G'' + \gamma G'C' \tag{16}$$

$$P' + HH' = 2\gamma C'H' + \nu^*H'' \tag{17}$$

$$Sc\,HC' = \frac{1}{\nu^*}C'' + \frac{1}{\nu^{*2}}\gamma(C')^2 \tag{18}$$

Here, we refer to the nondimentional viscosity $\nu^* = \nu(z)/\nu(\infty)$, and to the nondimensional diffusivity $D^* = D(z)/D(\infty)$. We assume that the Stokes-Einstein equation is strictly valid, which implies that $D^*\nu^* = 1$ and that $d\nu^*/dC$ is constant. The bulk Schmidt number, Sc, and the sensitivity factor γ, define the slope of the viscosity profile close to the electrode surface.

Boundary conditions for F, G and H are $F = H = P = G = 0$, $C = 1$ when $z = 0$, $F = H' = C = 0$, $G = -1$ when $z \longrightarrow \infty$.

Figure 1 shows the non-dimensional viscosity and velocity profiles obtained by numerical integration of Eqs. (14–18) and used in the four cases of the stability analysis presented in this work. Curves No. 1 refer to fluids with constant viscosity; Curves No. 2, refer to fluids with viscosity profiles obtained with $Sc = 50$ and $\gamma = 1$, and show a decay of the viscosity to the bulk value at $z = 1.0$ approximately. Curves No. 3 and 4 refer to fluids with viscosity profiles obtained with $\gamma = 1$, and $Sc = 1000$ and $Sc = 2000$ respectively, and show a decay of the viscosity to the bulk value at $z = 0.3$ approximately. These viscosity profiles follow a trend similar to the one of the concentration profile of $\mathbf{Fe}^{++}$, which is produced at the interface by the electrodissolution (Calabrese Barton and West, 2001).

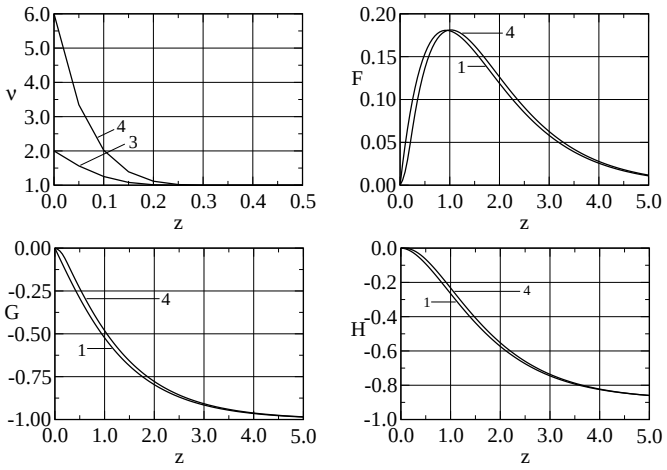

Figure 1: Dimensionless viscosity, ν, and velocity profiles F, G and H. Curves No. 1 refer to constant viscosity fluids. Curves No. 2, 3 and 4, to variable viscosity fluids. Curves No. 2: $Sc = 50$; Curves No. 3: $Sc = 1000$; Curves No. 4: $Sc = 2000$.($\gamma = 1$)

3. Perturbations of the Base State

We turn now to the question of the stability of the steady configurations of the hydrodynamic field described in Sec. (2), with respect to infinitesimally small disturbances.

Variables are made non-dimensional as follows: radial and axial coordinates are divided by the reference length $(\nu(\infty)/\Omega)^{1/2}$, velocity components are divided by the reference velocity $r_e\Omega$, pressure is divided by the reference pressure $\rho(r_e\Omega)^2$, viscosity is divided by the bulk value, $\nu(\infty)$ and time and the eigenvalue of the linearized problem are divided by the time required by a particle, turning with the azimuthal velocity $r_e\Omega^2$, to move a distance equal to the reference length, $(\nu(\infty)/\Omega)^{1/2}$. Here, r_e is the dimensional coordinate along the radial direction where the stability analysis is made. We define also the Reynolds number by the relation:

$$R = r_e \left(\frac{\Omega}{\nu(\infty)} \right)^{1/2} \tag{19}$$

The nondimensional concentration is defined by

$$c^* = \frac{C_T - C_\infty}{C_S - C_\infty}$$

where C_S and C_∞ are the saturation and bulk concentrations of the relevant chemical species.

Therefore, dropping the asterisks, the equations in nondimensional form are given by

$$\mathbf{div}\,\mathbf{v} = 0 \tag{20}$$

$$\frac{\partial \mathbf{v}}{\partial t} + \mathbf{v}\,\mathbf{grad}\,\mathbf{v} = -\frac{2}{R}\mathbf{e}_z \times \mathbf{v} - \mathbf{grad}\,p + \frac{1}{R}\,\mathbf{div}\,\tau \tag{21}$$

$$\frac{\partial c}{\partial t} + \mathbf{v} \cdot \mathbf{grad}\,c = \frac{1}{R\,Sc}\,\mathbf{div}\,(D\,\mathbf{grad}\,c) \tag{22}$$

The hidrodynamic field is written in the form of the von Kármán solution plus a perturbation. The steady and perturbation variables are identified with a bar and a tilde, respectively. Therefore

$$\begin{array}{llll} v_r = \bar{v}_r + \tilde{v}_r & v_\theta = \bar{v}_\theta + \tilde{v}_r & v_z = \bar{v}_r + \tilde{v}_z & \\ p = \bar{p} + \tilde{p} & C_T = \bar{c} + \tilde{c} & & \end{array}$$

The perturbed variables are introduced in the evolution equations. Subtracting the steady state solution, and neglecting the nonlinear terms containing products of the perturbations, the small amplitude perturbations evolution equations are given by

$$\frac{1}{r}\frac{\partial}{\partial r}(r\tilde{v}_r) + \frac{1}{r}\frac{\partial \tilde{v}_\theta}{\partial \theta} + \frac{\partial \tilde{v}_z}{\partial z} = 0 \tag{23}$$

$$\frac{\partial \tilde{v}_r}{\partial t} + \bar{v}_r\frac{\partial \tilde{v}_r}{\partial r} + \tilde{v}_r\frac{\partial \bar{v}_r}{\partial r} + \frac{\bar{v}_\theta}{r}\frac{\partial \tilde{v}_r}{\partial \theta} - 2\frac{\bar{v}_\theta \tilde{v}_\theta}{r} + \bar{v}_z\frac{\partial \tilde{v}_r}{\partial z} + \tilde{v}_z\frac{\partial \bar{v}_r}{\partial z} = 2\Omega v_\theta - \frac{1}{\rho}\frac{\partial \tilde{p}}{\partial r} +$$

$$\frac{1}{\rho}\left(\frac{1}{r}\frac{\partial}{\partial r}\left(r\tilde{\tau}_{rr}\right)+\frac{1}{r}\frac{\partial\tilde{\tau}_{r\theta}}{\partial\theta}-\frac{\tilde{\tau}_{\theta\theta}}{r}+\frac{\partial\tilde{\tau}_{rz}}{\partial z}\right) \tag{24}$$

$$\frac{\partial\tilde{v}_\theta}{\partial t}+\bar{v}_r\frac{\partial\tilde{v}_\theta}{\partial r}+\tilde{v}_r\frac{\partial\bar{v}_\theta}{\partial r}+\frac{\bar{v}_\theta}{r}\frac{\tilde{v}_\theta}{\partial\theta}+\frac{\bar{v}_r\tilde{v}_\theta+\tilde{v}_r\bar{v}_\theta}{r}+\bar{v}_z\frac{\partial\tilde{v}_\theta}{\partial z}+\tilde{v}_z\frac{\partial\bar{v}_\theta}{\partial z}=-2\Omega v_r-\frac{1}{\rho r}\frac{\partial\tilde{p}}{\partial\theta}+$$
$$\frac{1}{\rho}\left(\frac{1}{r^2}\frac{\partial}{\partial r}\left(r^2\tilde{\tau}_{r\theta}\right)+\frac{1}{r}\frac{\partial\tilde{\tau}_{\theta\theta}}{\partial\theta}+\frac{\partial\tilde{\tau}_{\theta z}}{\partial z}\right) \tag{25}$$

$$\frac{\partial\tilde{v}_z}{\partial t}+\bar{v}_r\frac{\partial\tilde{v}_z}{\partial r}+\frac{\bar{v}_\theta}{r}\frac{\partial\tilde{v}_z}{\partial\theta}+\bar{v}_z\frac{\partial\tilde{v}_z}{\partial z}+\tilde{v}_z\frac{\partial\bar{v}_z}{\partial z}=-\frac{1}{\rho}\frac{\partial\tilde{p}}{\partial z}+$$
$$\frac{1}{\rho}\left(\frac{1}{r}\frac{\partial}{\partial r}\left(r\tilde{\tau}_{rz}\right)+\frac{1}{r}\frac{\partial\tilde{\tau}_{\theta z}}{\partial\theta}+\frac{\partial\tilde{\tau}_{zz}}{\partial z}\right) \tag{26}$$

$$\frac{\partial\tilde{c}}{\partial t}+\bar{v}_r\frac{\partial\tilde{c}}{\partial r}+\frac{\bar{v}_\theta}{r}\frac{\partial\tilde{c}}{\partial\theta}+\bar{v}_z\frac{\partial\tilde{c}}{\partial z}+\tilde{v}_z\frac{d\bar{c}}{dz}=\bar{D}\left(\frac{1}{r}\frac{\partial}{\partial r}\left(r\frac{\partial\tilde{c}}{\partial r}\right)+\frac{1}{r}\frac{\partial}{\partial\theta}\left(\frac{1}{r}\frac{\partial\tilde{c}}{\partial\theta}\right)+\frac{\partial^2\tilde{c}}{\partial z^2}\right)+$$
$$\frac{d\bar{D}}{dz}\frac{\partial\tilde{c}}{\partial z}+\tilde{D}\frac{\partial^2\bar{c}}{\partial z^2}+\frac{\partial\tilde{D}}{\partial z}\frac{d\bar{c}}{dz} \tag{27}$$

Expanding the stress tensor components and simplifying using the continuity equation, results in

$$\frac{1}{r}\frac{\partial}{\partial r}(r\tilde{v}_r)+\frac{1}{r}\frac{\partial\tilde{v}_\theta}{\partial\theta}+\frac{\partial\tilde{v}_z}{\partial z}=0 \tag{28}$$

$$\frac{\partial\tilde{v}_r}{\partial t}+\bar{v}_r\frac{\partial\tilde{v}_r}{\partial r}+\tilde{v}_r\frac{\partial\bar{v}_r}{\partial r}+\frac{\bar{v}_\theta}{r}\frac{\partial\tilde{v}_r}{\partial\theta}-2\frac{\bar{v}_\theta\tilde{v}_\theta}{r}+\bar{v}_z\frac{\partial\tilde{v}_r}{\partial z}+\tilde{v}_z\frac{\partial\bar{v}_r}{\partial z}=2\frac{\tilde{v}_\theta}{R}-\frac{\partial\tilde{p}}{\partial r}+$$
$$\frac{1}{R}\left[\bar{\nu}\left(\frac{\partial^2\tilde{v}_r}{\partial r^2}+\frac{1}{r^2}\frac{\partial^2\tilde{v}_r}{\partial\theta^2}+\frac{\partial^2\tilde{v}_r}{\partial z^2}+\frac{1}{r}\frac{\partial\tilde{v}_r}{\partial r}-\frac{2}{r^2}\frac{\partial\tilde{v}_\theta}{\partial\theta}-\frac{\tilde{v}_r}{r^2}\right)+\frac{d\bar{\nu}}{dz}\left(\frac{\partial\tilde{v}_z}{\partial r}+\frac{\partial\tilde{v}_r}{\partial z}\right)+\right.$$
$$\left.\tilde{\nu}\left(\frac{\partial^2\bar{v}_r}{\partial z^2}+\frac{1}{r}\frac{\partial\bar{v}_r}{\partial r}-\frac{\bar{v}_r}{r^2}\right)+2\frac{\partial\bar{v}_r}{\partial r}\frac{\partial\tilde{\nu}}{\partial r}+\frac{\partial\tilde{\nu}}{\partial z}\frac{\partial\bar{v}_r}{\partial z}\right] \tag{29}$$

$$\frac{\partial\tilde{v}_\theta}{\partial t}+\bar{v}_r\frac{\partial\tilde{v}_\theta}{\partial r}+\tilde{v}_r\frac{\partial\bar{v}_\theta}{\partial r}+\frac{\bar{v}_\theta}{r}\frac{\partial\tilde{v}_\theta}{\partial\theta}+\frac{\bar{v}_r\tilde{v}_\theta+\tilde{v}_r\bar{v}_\theta}{r}+\bar{v}_z\frac{\partial\tilde{v}_\theta}{\partial z}+\tilde{v}_z\frac{\partial\bar{v}_\theta}{\partial z}=-2\frac{\tilde{v}_r}{R}-\frac{1}{r}\frac{\partial\tilde{p}}{\partial\theta}+$$
$$\frac{1}{R}\left[\bar{\nu}\left(\frac{\partial^2\tilde{v}_\theta}{\partial r^2}+\frac{1}{r^2}\frac{\partial^2\tilde{v}_\theta}{\partial\theta^2}+\frac{\partial^2\tilde{v}_\theta}{\partial z^2}+\frac{1}{r}\frac{\partial^2\tilde{v}_\theta}{\partial r}+\frac{2}{r^2}\frac{\partial\tilde{v}_r}{\partial\theta}-\frac{\tilde{v}_\theta}{r^2}\right)+\frac{d\bar{\nu}}{dz}\left(\frac{1}{r}\frac{\partial\tilde{v}_z}{\partial\theta}+\frac{\partial\tilde{v}_\theta}{\partial z}\right)+\right.$$
$$\left.\tilde{\nu}\left(\frac{\partial^2\bar{v}_\theta}{\partial z^2}+\frac{1}{r}\frac{\partial\bar{v}_\theta}{\partial r}-\frac{\bar{v}_\theta}{r^2}\right)+\frac{2\bar{v}_r}{r^2}\frac{\partial\tilde{\nu}}{\partial\theta}+\frac{\partial\tilde{\nu}}{\partial z}\frac{\partial\bar{v}_\theta}{\partial z}\right] \tag{30}$$

$$\frac{\partial\tilde{v}_z}{\partial t}+\bar{v}_r\frac{\partial\tilde{v}_z}{\partial r}+\tilde{v}_r\frac{\partial\bar{v}_z}{\partial r}+\frac{\bar{v}_\theta}{r}\frac{\partial\tilde{v}_z}{\partial\theta}+\bar{v}_z\frac{\partial v_z}{\partial z}+\tilde{v}_z\frac{\partial\bar{v}_z}{\partial z}=-\frac{\partial\tilde{p}}{\partial z}+$$
$$\frac{1}{R}\left[\bar{\nu}\left(\frac{\partial^2\tilde{v}_z}{\partial r^2}+\frac{1}{r^2}\frac{\partial^2\tilde{v}_z}{\partial\theta^2}+\frac{\partial^2\tilde{v}_z}{\partial z^2}+\frac{1}{r}\frac{\partial\tilde{v}_z}{\partial r}\right)+2\frac{d\bar{\nu}}{dz}\frac{\partial v_z}{\partial z}\right.$$
$$\left.2\tilde{\nu}\frac{\partial^2\bar{v}_z}{\partial z^2}+\frac{\partial\tilde{\nu}}{\partial r}\left(\frac{\partial\bar{v}_z}{\partial r}+\frac{\partial\bar{v}_r}{\partial z}\right)+\frac{1}{r}\frac{\partial\tilde{\nu}}{\partial\theta}\left(\frac{\partial\bar{v}_\theta}{\partial z}+\frac{1}{r}\frac{\partial\bar{v}_z}{\partial\theta}\right)+2\frac{\partial\tilde{\nu}}{\partial z}\frac{\partial\bar{v}_z}{\partial z}\right] \tag{31}$$

$$\frac{\partial\tilde{c}}{\partial t}+\bar{v}_r\frac{\partial\tilde{c}}{\partial r}+\frac{\bar{v}_\theta}{r}\frac{\partial\tilde{c}}{\partial\theta}+\bar{v}_z\frac{\partial\tilde{c}}{\partial z}+\tilde{v}_z\frac{d\bar{c}}{dz}=\frac{1}{R\,Sc}\left[\bar{D}\left(\frac{1}{r}\frac{\partial}{\partial r}\left(r\frac{\partial\tilde{c}}{\partial r}\right)+\frac{1}{r}\frac{\partial}{\partial\theta}\left(\frac{1}{r}\frac{\partial\tilde{c}}{\partial\theta}\right)+\frac{\partial^2\tilde{c}}{\partial z^2}\right)+\right.$$
$$\left.\frac{d\bar{D}}{dz}\frac{\partial\tilde{c}}{\partial z}+\tilde{D}\frac{d^2\bar{c}}{dz^2}+\frac{\partial\tilde{D}}{\partial z}\frac{\partial\bar{c}}{\partial z}\right] \tag{32}$$

The perturbed field is assumed as

$$\begin{pmatrix}v_r\\v_\theta\\v_z\\p\\C_T\end{pmatrix}=\begin{pmatrix}r\Omega F\\r\Omega G\\(\nu(\infty)\Omega)^{1/2}H\\\rho\nu(\infty)\Omega P\\C_\infty+(C_s-C_\infty)\,C\end{pmatrix}+A\begin{pmatrix}r_e\Omega\,f\\r_e\Omega\,g\\r_e\Omega\,h\\\rho\nu(\infty)\Omega\,\pi\\C_\infty+(C_s-C_\infty)\,c\end{pmatrix}\exp\left[i(\alpha r+\beta R\theta-\omega t)\right]+cc \tag{33}$$

where C and c are functions of z. Re-writing the variables in Eq. (33) in nondimensional form, the perturbed non-dimensional velocity components, pressure, and concentration are written as:

$$\begin{pmatrix}v_r\\v_\theta\\v_z\\p\\C_T^*\end{pmatrix}=\begin{pmatrix}rF/R\\rG/R\\H/R\\p/R^2\\C\end{pmatrix}+A\begin{pmatrix}f\\g\\h\\\pi\\c\end{pmatrix}\exp\left[i(\alpha r+\beta R\theta-\omega t)\right]+cc \tag{34}$$

where ω is a complex number, with $\Re(\omega)$ and $\Im(\omega)$ being, respectively, the frequency and the rate of growth of the perturbation. Parameters α and β are the components of the perturbation wave-vector along the radial and azimuthal directions. For a given time, the phase of the perturbation is constant along branches of a logarithmic spiral, with the branches curved in the clockwise direction if β/α is positive and counter-clockwise, if negative. The structure turns counter-clockwise if ω/β is positive and clockwise, if negative.

Perturbation and steady state variables are introduced in the evolution equations, resulting in

$$i\left(\alpha-\frac{i}{r}\right)f+i\frac{R}{r}\beta g+h'=0 \tag{35}$$

$$\begin{aligned}i\left(\frac{r}{R}\alpha F+\beta G-\omega\right)f+\frac{r}{R}F'h+i\alpha\pi-\frac{r}{R}F'\gamma c'-\frac{r}{R}F''\gamma c=\frac{1}{R}\Bigg(\nu f''-\\ \nu\left(\alpha^2+\frac{R^2}{r^2}\beta^2\right)f-Ff+2(G+1)g-Hf'+i\alpha\nu'h+\nu'f'+2i\alpha F\gamma c\Bigg)+\\ \frac{1}{R^2}\left(i\frac{R}{r}\nu\alpha f-2\,i\frac{R^2}{r^2}\nu\beta g\right)-\frac{\nu}{Rr^2}f\end{aligned} \tag{36}$$

$$\begin{aligned}i\left(\frac{r}{R}\alpha F+\beta G-\omega\right)g+\frac{r}{R}G'h+i\frac{R}{r}\beta\pi-\frac{r}{R}\left(G''\gamma c+G'\gamma c'\right)=\frac{1}{R}\left(\nu g''-\right.\\ \nu\left(\alpha^2+\frac{R^2}{r^2}\beta^2\right)g-Fg-2(G+1)f-Hg'+i\frac{R}{r}\beta\nu'h+\nu'g'+\frac{2R}{r}i\beta F\gamma c\Bigg)+\\ \frac{1}{R^2}\left(i\frac{R}{r}\nu\alpha g-2\,i\frac{R^2}{r^2}\nu\beta f\right)-\frac{\nu}{Rr^2}g\end{aligned} \tag{37}$$

$$\begin{aligned}i\left(\frac{r}{R}\alpha F+\beta G-\omega\right)h+\pi'-i\beta\;G'\gamma c-\frac{r}{R}i\alpha F'\gamma c=\frac{1}{R}\Bigg(\nu h''-\nu\left(\alpha^2+\frac{R^2}{r^2}\beta^2\right)h-\\ Hh'-H'h+2\nu'h'+2H''\gamma c+2H'\gamma c'\Bigg)+\frac{i}{Rr}\,\nu\alpha h\end{aligned} \tag{38}$$

$$\begin{aligned}i\left(\frac{r}{R}\alpha F+\beta G-\omega\right)c+C'h=\frac{1}{R\,Sc\,\bar\nu}\Bigg(-\left(\alpha\bar\alpha+\frac{R^2}{r^2}\beta^2\right)c+\\ \frac{1}{\bar\nu}\left(\left(2\frac{\bar\nu'}{\bar\nu}\gamma-\gamma'\right)C'-\gamma C''\right)c-\left(\frac{\bar\nu'}{\bar\nu}+\frac{1}{\bar\nu}C'\gamma+Sc\,\bar\nu H\right)c'+c''\Bigg)\end{aligned} \tag{39}$$

Introducing the parallel flow hypothesis, eliminating the pressure, and dropping terms of order R^{-2}, leads to:

$$\begin{aligned}\Big(i\nu\left(D^2-\lambda^2\right)\left(D^2-\bar\lambda^2\right)+i\nu'D\left(2D^2-\lambda^2-\bar\lambda^2\right)+i\nu''\left(D^2+\bar\lambda^2\right)+\\ R\left(\alpha F+\beta G-\omega\right)\left(D^2-\bar\lambda^2\right)-R\left(\bar\alpha F''+\beta G''\right)-iHD\left(D^2-\bar\lambda^2\right)-\\ iH'\left(D^2-\bar\lambda^2\right)-iFD^2\Big)h+\left(2\left(G+1\right)D+\;2G'\right)\eta+\Big(R\left(\bar\alpha F'+\beta G'\right)\gamma D^2+\\ \Big(2R\left(\bar\alpha F''+\beta G''\right)+6i\bar\lambda^2F\Big)\gamma D+\Big(R\bar\lambda^2\left(\alpha F'+\beta G'\right)+R\left(\bar\alpha F'''+\beta G'''\right)+\\ 6i\bar\lambda^2F'\Big)\gamma+\Big(R\left(\bar\alpha F''+\beta G''\right)+6i\bar\lambda^2F\Big)\gamma'\Big)c=0\end{aligned} \tag{40}$$

$$\begin{aligned}\left(2\left(G+1\right)D-iR\left(\alpha G'-\beta F'\right)\right)h+\Big(i\nu\left(D^2-\lambda^2\right)+i\nu'D+R\left(\alpha F+\beta G-\omega\right)-\\ iHD-iF\Big)\eta+iR\left(\alpha G'-\beta F'\right)\gamma c'+iR\alpha G''\gamma c=0\end{aligned} \tag{41}$$

$$\begin{aligned}R\,Sc\,i\left(\alpha F+\beta G-\omega\right)c+R\,Sc\,C'h-\frac{1}{\bar\nu}\Bigg(-\bar\lambda^2+\frac{1}{\bar\nu}\left(\left(2\frac{\bar\nu'}{\bar\nu}\gamma-\gamma'\right)C'-\gamma C''\right)c+\\ \left(\frac{\bar\nu'}{\bar\nu}+\frac{1}{\bar\nu}C'\gamma+Sc\,\bar\nu H\right)c'+c''\Bigg)=0\end{aligned} \tag{42}$$

Eqs. (40 to 42) can be re-written as $A\mathbf{X}=\omega R\,B\mathbf{X}$:

$$\begin{pmatrix}A_{11}&A_{12}&A_{13}\\A_{21}&A_{22}&A_{23}\\A_{31}&&A_{33}\end{pmatrix}\begin{pmatrix}h\\\eta\\c\end{pmatrix}\;=\;\omega R\begin{pmatrix}B_{11}&&\\&B_{22}&\\&&B_{33}\end{pmatrix}\begin{pmatrix}h\\\eta\\c\end{pmatrix} \tag{43}$$

where the missing elements in the above matrices are null and the operators A_{ij} and B_{ij} are given by:

$$\begin{aligned}&A_{11}=a_{114}D^4+a_{113}D^3+a_{112}D^2+a_{111}D+a_{110} && A_{12}=a_{121}D+a_{120} && A_{13}=a_{132}D^2+a_{131}D+a_{130}\\&A_{21}=a_{211}D+a_{210} && A_{22}=a_{222}D^2+a_{221}D+a_{220} && A_{23}=a_{231}D+a_{230}\\&A_{31}=a_{310} && && A_{33}=a_{332}D^2+a_{331}D+a_{330}\\&B_{11}=D^2-\bar\lambda^2 && B_{22}=1 && B_{33}=iSc\end{aligned}$$

with coefficients given by:

$$a_{114} = i\nu \qquad a_{113} = i(2\nu' - H) \qquad a_{112} = i\nu'' - i\nu\left(\lambda^2 + \bar{\lambda}^2\right) + R\left(\alpha F + \beta G\right) - i\left(H' + F\right)$$

$$a_{111} = -i\nu'\left(\lambda^2 + \bar{\lambda}^2\right) + iH\bar{\lambda}^2 \qquad a_{110} = i\bar{\lambda}^2\left(\nu'' + \nu\lambda^2\right) - R\left(\alpha F + \beta G\right)\bar{\lambda}^2 - R\left(\bar{\alpha}F'' + \beta G''\right) + iH'\bar{\lambda}^2$$

$$a_{121} = 2\left(G + 1\right) \qquad a_{120} = 2G'$$

$$a_{132} = R\left(\bar{\alpha}F' + \beta G'\right)\gamma \qquad a_{131} = \left[2R\left(\bar{\alpha}F'' + \beta G''\right) + 6i\bar{\lambda}^2 F\right]\gamma$$

$$a_{130} = \left(R\bar{\lambda}^2\left(\alpha F' + \beta G'\right) + R\left(\bar{\alpha}F''' + \beta G'''\right) + 6i\bar{\lambda}^2 F'\right)\gamma + \left(R\left(\bar{\alpha}F'' + \beta G''\right) + 6i\bar{\lambda}^2 F\right)\gamma'$$

$$a_{211} = 2\left(G + 1\right) \qquad a_{210} = -iR\left(\alpha G' - \beta F'\right)$$

$$a_{222} = i\nu \qquad a_{221} = i\left(\nu' - H\right) \qquad a_{220} = -i\nu\lambda^2 + R\left(\alpha F + \beta G\right) - iF$$

$$a_{231} = iR\left(\alpha G' - \beta F'\right)\gamma \qquad a_{230} = iR\alpha G''\gamma \qquad a_{310} = R\,Sc\,C'$$

$$a_{332} = -\frac{1}{\bar{\nu}} \qquad a_{331} = \frac{1}{\bar{\nu}}\left(\frac{\bar{\nu}'}{\bar{\nu}} + \frac{1}{\bar{\nu}}C'\gamma + Sc\,\bar{\nu}H\right)$$

$$a_{330} = iR\,Sc\left(\alpha F + \beta G\right) - \frac{1}{\bar{\nu}}\left(-\bar{\lambda}^2 + \frac{1}{\bar{\nu}}\left(\left(2\frac{\bar{\nu}'}{\bar{\nu}}\gamma - \gamma'\right)C' - \gamma C''\right)\right)$$

Boundary conditions of the problem require non-slip flow and vanishing axial component of the velocity at the electrode surface. These conditions are already fulfilled by the base-state, so the hydrodynamic field cannot be modified by the perturbation at the electrode surface. In consequence we must require $g = h = c = 0$ in $\xi = 0$. Moreover, we conclude from Eq. (35) that $h' = 0$ at the electrode surface. In $\xi \longrightarrow \infty$ we require that the perturbation vanishes ($g = h = c = 0$) and that $h' = 0$. Eq. (43) defines a generalized eigenvalue/eigenfunction

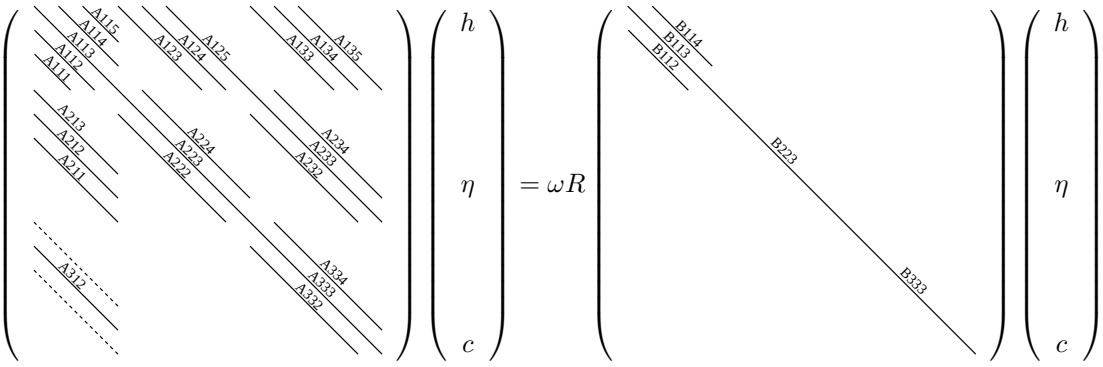

Figure 2: Structure of the operators of the discrete eigenvale-eigenvector problem.

problem. The eigenfunctions are the normal modes of the model, the imaginary and real parts of each eigenvalue being, respectively, the rate of growth and the angular velocity of the perturbation relative to the angular velocity of the disk. The matrix structure of the operators of the discrete eigenvale-eigenvector problem is shown in Figure 2

The parameter space of the problem contains *five* variables: the Reynolds number, the Schmidt number, the sensitivity parameter γ, and the perturbation wavevector components α and β.

4. Results

The effect of viscosity stratification is analyzed by comparing stability properties of constant viscosity fluids with the properties of the variable viscosity configuration discussed in Sec. (2).

The results are summarized in Fig. 3 and Table 1. Figure 3 shows the neutral stability curves.

The neutral curves were evaluated in domains with length $z_{max} = 40$, using grids with 801 uniformly spaced points. Larger domains do not significantly affect the presented results.

Curves No. 1 in Figs. 3 refer to constant viscosity fluids ($\gamma = 0$), the remaining ones, to variable viscosity fluids: Curves Nos. 2 refer to $Sc = 5$, Curves Nos. 3 refer $Sc = 1000$, and Curves Nos. 4 to fluids with $Sc = 2000$, respectively, obtained with $\gamma = 1$.

The curves shown in fig. 3 are relative to stationary disturbances ($\omega_r = 0$) and represent an extension of Malik's (Malik, 1986) work by including the variable viscosity cases.

These results must be interpreted as preliminary, as the accuracy of the simulations was not completely assessed, specially for the Curves Nos. 3 - 4 (high Schmidt number simulations), where the boundary layer thickness is very small. We believe, however, that the results are qualitatively correct.

Curves Nos. 2 - 4 show a large reduction on the critical Reynolds number for the cases of viscosity varying with the concentration field ($\gamma \neq 0$). Even though the steady state profiles (Fig. 1) are not appreciably affected by the viscosity variations, the stability of the flow is dramatically affected by the coupling of the chemical species troought the viscosity field.

Figure 3 shows that the main factor affecting the critical Reynolds number of a neutral curve is the Schmidt number, Sc, which defines the thickness of the layer in which the viscosity varies. As a rule, thicker layers lead to smaller reductions. The above results are, qualitatively, in agreement with the experimental ones. Indeed, the system becomes more unstable as the angular velocity of the electrode increases, and more stable as the bulk viscosity increases, with addition of glycerol.

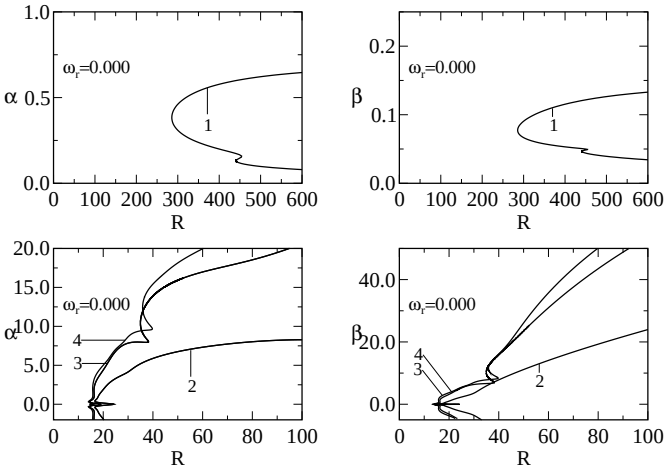

Figure 3: Neutral curves for constant and variable viscosity fluids. Curves No. 1 refer to constant viscosity fluids. Curves No. 2, 3 and 4, to variable viscosity fluids. Curves No. 2: $Sc = 50$; Curves No. 3: $Sc = 1000$; Curves No. 4: $Sc = 2000$.($\gamma = 1$)

A quantitative comparison of the effect of the Schmidt and sensitivity factor γ can be done observing the coordinates of the critical points, below which no stationary perturbations are amplified, for the four studied configurations, as shown in Table I.

Table 1: Coordinates of the critical points

Curve	Sc	γ	R	α	β
1	0	0	285.4	0.3818	0.0771
2	50	1	16.6	0.3986	0.1278
3	1000	1	14.5	0.3647	0.1336
4	2000	1	14.2	0.3427	0.1043

While the values of α and β are not strongly affected by Sc and γ, the critical Reynolds number has a very large drop, being more than one order of magnitude smaller for $\gamma = 1$ than for the case $\gamma = 0$. The Schmidt number has a moderate effect, reducing the critical Reynolds number as Sc increases from 50 to 2000 for a fixed value of γ.

5. Conclusions

In this work we analyzed the behavior of the most unstable modes in rotating disk flow with a stratified viscosity depending on the concentration of a chemical species transported by the flow, and compared the results with existing results for the constant viscosity case.

The main conclusions of this work may be summarized as follows:

1. The proposed coupled hydrodynamic-chemistry model, with a stratified viscosity profile depending on the concentration of the chemical species, shows that, in all cases considered, the system becomes more unstable as the thickness of the layer where the viscosity varies decreases.

2. The reduction in teh stability of the flow is more pronounced for liquids, where the Schmidt number is of order of 10^3 than for gases, where it falls in the range of 10.

6. Acknowledgements

The authors acknowledge prof. Antônio Castelo Filho (USP-S.Carlos), who developed the numerical code using the Continuation Method to evaluate the neutral stability curves presented in this work. Fruitful discussions with profs. R. E. Kelly from the University of California at Los Angeles and D. Walgraef from the Free University of Brussels are also acknowledged. J. P. received financial support from FAPERJ (Brazil). N. M. acknowledges financial support from CNPq (Brazil).

7. References

Barcia, O. E., Mattos, O. R., and Tribollet, B., 1992, Anodic dissolution of iron in acid sulfate under mass transport control, "J. Eletrochem. Soc.", Vol. 139, pp. 446–453.

Calabrese Barton, S. and West, A. C., 2001, Electrohydrodynamic Impedance in the Presence of Nonuniform Transport Properties, "J. of the Electrochemical Soc.", Vol. 148-4, pp. A381–A387.

Epelboin, I., Gabrielli, G., Keddam, M., Lestrach, J. C., and Takenouti, H., 1979, Passivation of Iron in Sulfuric acid Medium, "J. Eletrochem. Soc.", Vol. 126, pp. 1632–1637.

Faller, A. J., 1991, Instability and Transition of the Disturbed Flow Over a Rotating Disk, "J. Fluid Mech.", Vol. 230, pp. 245–269.

Ferreira, J. R. R. M., Barcia, O. E., and Tribollet, B., 1994, Iron dissolution under mass transport control: the effect of viscosity on the current oscillation, "Eletrochim. Acta", Vol. 39, pp. 933–938.

Geraldo, A. B., Barcia, O. E., Mattos, O. R., Huet, F., and Tribollet, B., 1998, New results concerning the oscillations observed for the system iron-sulphuric acid, "Electrochim. Acta", Vol. 44, pp. 455–465.

Levich, V. G., 1962, "Physicochemical Hydrodynamics", Prentice Hall, Englewood Cliffs, NJ.

Lingwood, R. J., 1995, Absolute instability of the boundary layer on a rotating disk, "J. Fluid Mech.", Vol. 299, pp. 17–33.

Malik, M. R., 1986, The Neutral Curve for Stationary Disturbances in Rotating-disk Flow, "J. Fluid Mech.", Vol. 164, pp. 275–287.

Pontes, J., Mangiavacchi, N., Conceição, A. R., Barcia, O. E., Mattos, O. E., and Tribollet, B., 2002, Instabilities in Electrtochemical Systems with a Rotatinng Disk electrode, "J. of the Braz. Soc. of Mechanical Sciences", Vol. XXIV-3, pp. 139–148.

Pontes, J., Mangiavacchi, N., Conceição, A. R., Barcia, O. E., Mattos, O. E., and Tribollet, B., 2004, Rotating Disk Flow Stability in Electrochemical Cells: Effect of Viscosity Stratification, "Phys. Fluids", Vol. 16, No. 3, pp. 707–716.

Reed, H. L. and Saric, W. S., 1989, Stability of Three-Dimensional Boundary Layers, "Ann. Rev. Fluid Mech.", Vol. 21, pp. 235–84.

Russel, P. and Newman, J., 1986, Current oscillations observed within the limiting current plateau for iron in sulfuric acid, "J. Eletrochem. Soc.", Vol. 133, pp. 2093–2097.

Schäfer, P., Severin, J., and Herwin, H., 1995, The effect of heat transfer on the stability of laminar boundary layers, "Int. J. Heat Mass Transfer", Vol. 38-10, pp. 1855–1863.

Schlichting, H. and Gersten, K., 1999, "Boundary Layer Theory", Springer, Berlin.

Tribollet, B. and Newman, J., 1983, The modulated flow at a rotating disk electrode, "J. Eletrochem. Soc.", Vol. 130, pp. 2016–2026.

Turkyilmazoglu, M., Cole, J. W., and Gajjar, J. S. B., 1998, Absolute and Convective Instabilities in the Compressible Boundary Layer on a Rotating Disk, CLSCM Report CLSCM-1998-001, University of Manchester, Manchester.

von Kármán, T. and Angew, Z., 1921, Uber Laminare und Turbulente Reibung, "Math. Mec.", Vol. 1, pp. 233–252.